Longitudinal oscillation of a liquid sheet by parallel air flows

Oshima, Ippei

Sou, Akira

(Citation)
International Journal of Multiphase Flow,110:179-188

(Issue Date)
2019-01

(Resource Type)
journal article

(Version)
Accepted Manuscript

Longitudinal Oscillation of a Liquid Sheet by Parallel Air Flows

Ippei Oshima[*1], Akira Sou[*2]

*1 Ph. D. Student, Graduate School of Maritime Sciences, Kobe University, Kobe-shi, Hyogo-ken, 658-0022, Japan, E-mail: 134w102w@stu.kobe-u.ac.jp.

*2 Professor, Graduate School of Maritime Sciences, Kobe University, Kobe-shi, Hyogo-ken, 658-0022, Japan, E-mail: sou@maritime.kobe-u.ac.jp.

Keywords: Gas turbine, Air-blast atomizer, Liquid sheet, Visualization, Lip thickness, Longitudinal wavelength

Abstract

A liquid fuel sheet injected into the combustor of gas turbine engines is deformed and atomized by the complex interactions between the liquid sheet and air flows. Aiming at improving the control technology of a fuel spray, the oscillation phenomenon and the primary break-up process of a planar liquid sheet with air flows have been studied for many years. Based on the previous studies, we propose a new correlation on the longitudinal wavelength λ_{Lon} given by $\frac{\lambda_{Lon}}{D_{Lip}} = \frac{c}{\sqrt{MR_{Lip}}}$ and that on the oscillation frequency f_{Lon} of a liquid sheet given by $f_{Lon} = \frac{c' V_G}{\sqrt{\rho_L/\rho_G}\sqrt{D_L D_{Lip}}}$, where MR_{Lip} is the lip momentum ratio defined in this study. In addition to previous visualization experiments of a planar liquid sheet and parallel air flows with various densities of gas and liquid, gas and liquid velocities, liquid sheet thicknesses and lip thicknesses, we carry out an additional experiment with various gas velocities and liquid viscosities to cover all the effects of fluid properties, injector geometries including gas and liquid boundary layers on the deformation and the atomization characteristics of the oscillating liquid sheet. Image analysis is conducted to obtain f_{Lon}. As a result, we confirm that liquid viscosity does not affect f_{Lon} and λ_{Lon} of the liquid sheet in a wide range of liquid Reynolds number. Finally, we verify the validity of the correlations of λ_{Lon} whose constant c is 14.3 and f_{Lon} whose constant c' is 0.095.

1. Introduction

A gas turbine engine has been used for aircraft propulsion and power generation. An air-blast atomizer, in which an injected liquid sheet is atomized by high-speed air flows, is often used in gas turbines [1]. In spite of the importance of the fuel spray characteristics in a gas turbine combustor, the atomization phenomenon of the liquid film discharged from the injector has not been understood yet because of the complex multi-phase and multi-scale phenomena and the difficulty in observing the high-speed atomization process.

Therefore, the atomization and deformation process of a simple planar liquid sheet induced by air flows has been investigated. Squire [2] performed theoretical and experimental study about a flapping liquid film in a stationary

gas at sub atmospheric ambient pressures P_a and concluded that his theoretical prediction of the longitudinal wavelength λ_{Lon} of the liquid sheet oscillation agreed with his measured result. Stapper et al. [3] visualized a plane liquid sheet and proposed a deformation pattern map of a liquid sheet. Yoshida et al. [4] investigated the effects of the gas injection angle on the gas flow field and the droplet sizes. Fernandez et al. [5] carried out an experiment using water and kerosene as a liquid and measured the longitudinal oscillation frequency f_{Lon} of the liquid sheet. Dejean et al. [6] investigated the effects of liquid and air thicknesses on f_{Lon}. Villedieu et al. [7] performed numerical simulations using the SLOSH code, and compared the numerical and experimental results of gas velocity profile and break-up length. Li-zi et al. [8] proposed a break-up model and predicted the droplet sizes theoretically using Kelvin-Helmholtz (K-H) instability theory [9-10] without taking into account the effects of injector geometries.

Ligaments and bags are generated during the primary atomization of the liquid sheet. By knowing the longitudinal and transversal wavelengths of the liquid sheet, we can predict the characteristics of primary atomization, such as the sizes of ligaments and bags. The bag break-up generates small droplets, and the ligament break-up generates large droplets. Therefore, the longitudinal and transversal wavelengths are required to develop a break-up model based on the detailed break-up process.

The fabrication technology determines the minimum thickness of an atomizer lip. Excessively reducing the lip thickness may causes the destruction of the lip in the engine operation, while increase in the lip thickness strongly affects the initial deformation and the characteristics of primary atomization of the liquid fuel sheet, which may finally influence fuel spray diameter. Hence, in this study we clarify the effect of the lip thickness on the initial deformation characteristics of the liquid sheet.

The effects of fluid properties of gas and liquid and injector geometries as well as gas and liquid velocities and ambient pressures on f_{Lon} and λ_{Lon} have been discussed [5, 6, 11, 12]. Lozano et al. [11] investigated the effects of liquid and air thicknesses on λ_{Lon} of the planar liquid sheet, and proposed a correlation based on their experimental result. The present authors [12] investigated the effects of fluid properties and velocities of gas and liquid on the oscillating characteristics of the liquid sheet by two-dimensional numerical simulations. We clarified that the oscillation of a liquid sheet is suppressed by the atomizer lip which forms a wake in its downstream, and proposed a correlation on λ_{Lon}. Villermaux [13] and Marmottant & Villermaux [14] reported the importance of boundary layer on λ_{Lon}. In the previous studies, however, the effects of fluid properties and injector geometries on f_{Lon} and λ_{Lon} were discussed separately, and there are no correlations of f_{Lon} and λ_{Lon} for the air-blast atomizer which takes into account the effects of both fluid properties and injector geometries. Thus, new correlations on f_{Lon} and λ_{Lon} for the air-blast atomizer which takes into account the both effects must be developed. The present authors [15] conducted visualization experiments of a planar liquid sheet and air flows with various liquid densities ρ_L, gas densities ρ_G, liquid velocities V_L, gas velocities V_G, liquid sheet thicknesses D_L and lip thicknesses D_{Lip}, and presented empirical correlations on λ_{Lon} and f_{Lon}. However, the empirical correlations are not based on physical background and did not take into account the liquid velocity boundary layer.

In the present study, we examine the oscillation phenomenon of a liquid sheet based on the previous researches and propose a new correlation on λ_{Lon} and that on f_{Lon} of an oscillating liquid sheet induced by air flows by focusing on the gas and liquid boundary layers. Then, we carry out an additional visualization experiment of a

planar liquid sheet and parallel air flows with various liquid viscosities μ_L and gas velocities V_G to cover all the effects of fluid properties and the injector geometries on the deformation and atomization characteristics of the oscillating liquid sheet. Finally, the validities of the proposed correlations on λ_{Lon} and f_{Lon} are verified through the comparison of measured and estimated results.

2. Proposal of the correlations on the longitudinal wavelength and the oscillation frequency of the liquid sheet oscillation

In this section, firstly, we review some of the previous correlations on λ_{Lon}. Then, by taking into account the effect of the lip, we propose a new empirical correlation for an air-blast atomizer.

Some of the major correlations on λ_{Lon} of the oscillating liquid column and sheet are summarized in Table 1, where δ_G is the gas boundary layer thickness, σ the surface tension, ρ the density, V the inlet velocity, D the thickness, and the subscripts G, L and Lip are gas, liquid and lip, respectively. In the table, MFR is the momentum flux ratio defined by

$$\mathrm{MFR} = \frac{\rho_G {V_G}^2}{\rho_L {V_L}^2} \tag{1}$$

and MR is the momentum ratio defined by

$$\mathrm{MR} = \frac{\rho_G {V_G}^2 D_G}{\rho_L {V_L}^2 D_L} \tag{2}$$

These correlations were proposed through the theoretical, experimental, or numerical studies under various operating conditions and fuel injector designs [2, 11-14].

The viscous effect on the shear instability is generally small at high Reynolds number. Under low Reynolds number condition, in contrast, the gas viscous effect on the shear instability becomes effective because the ratio of the viscous diffusion timescale to the instability development timescale becomes small [16]. The effect of surface tension σ or gas boundary layer thickness δ_G at the interface for the liquid-gas coaxial jet on λ_{Lon} is individually taken into account in some correlations [13, 14]. Based on the inviscid linear instability analysis of a liquid sheet, Squire [2] takes surface tension effect into account in his correlation of λ_{Lon}. In contrast, surface tension effect on λ_{Lon} was not considered under the high Weber number or the thick boundary layer layer conditions [11, 12, 14]. Lozano et al. [11] proposed the following empirical correlation on λ_{Lon} through the experiments for various D_G and D_L:

$$\frac{\lambda_{Lon}}{\sqrt{D_L D_G}} = \frac{20.39}{\sqrt{MR}} \tag{3}$$

By inserting eq. (2) into eq. (3), we can derive the following equation:

$$\frac{\lambda_{Lon}}{D_L} = \frac{20.39}{\sqrt{MFR}} \tag{4}$$

which indicates that λ_{Lon} depends not on D_G but on D_L, if MFR is the key parameter. However, the effects of fluid properties of gas and liquid on λ_{Lon} were not investigated systematically in the previous studies, and we cannot understand the reason why the dominant length scale is D_L within various dominant length scales including D_{Lip}, δ_G and δ_L. Based on the numerical simulations with various V_G, V_L, ρ_L, ρ_G, μ_L and μ_G with constant D_L and D_{Lip}, the

present authors [12] proposed the following correlation on λ_{Lon} under the limited condition of constant D_L and D_{Lip}:

$$\lambda_{Lon} \propto \frac{1}{\sqrt{MFR}} \tag{5}$$

These correlations suggest that MFR is dominant for λ_{Lon} [11, 12].

Then, we discuss about which length scale should be used to non-dimensionalize λ_{Lon}. Some researchers use the boundary layer thickness δ at the gas-liquid interface to normalize λ_{Lon} [13, 14]. We derive the following correlation on λ_{Lon} normalized by δ:

$$\frac{\lambda_{Lon}}{\delta} \propto \frac{1}{\sqrt{MFR}} \tag{6}$$

We reported through a number of numerical simulations that a wake is formed downstream of the lip, which decreases the gas velocity gradient at the liquid sheet interface [12]. The result shows that the boundary layer thickness δ_G of the gas flow at the gas-liquid interface can be presented by the lip thickness D_{Lip}, and we can neglect the liquid boundary layer thickness δ_L because the formation of a liquid boundary layer requires much longer time than the deformation of a liquid sheet, which was clarified by Marmottant et al. [14]. Based on these considerations, eq. (6) can be rewritten as

$$\frac{\lambda_{Lon}}{\delta} \sim \frac{\lambda_{Lon}}{D_{Lip}} \propto \frac{1}{\sqrt{MFR}} \tag{7}$$

Here, we discuss about the length scales in momentums of gas and liquid. The momentum of a thin liquid film which exchanges the momentum with the surrounding air flow is clearly given by $\rho_L V_L^2 D_L$ because not the liquid shear layer whose thickness is δ_L along the gas-liquid interface but the entire liquid sheet oscillates whose thickness is D_L, while the dominant momentum of gas phase should not be $\rho_G V_G^2 D_G$ because not all the air flows injected from the injector but the air flow in the velocity boundary layer of the wake whose thickness is as large as the lip thickness D_{Lip} interacts with the liquid sheet. Therefore, we define the dominant momentum of gas phase as $\rho_G V_G^2 D_{Lip}$, and propose a new dimensionless number, the lip momentum ratio MR_{Lip}, which has a similar formulation with MR but using D_{Lip} as follows:

$$\mathrm{MR}_{Lip} = \frac{\rho_G {V_G}^2 D_{Lip}}{\rho_L {V_L}^2 D_L} \tag{8}$$

By replacing MFR in eq. (7) with MR_{Lip}, we introduce the following dimensionless correlation on λ_{Lon} based on the conclusions that (i) D_{Lip} should be used to normalize λ_{Lon}, and (ii) the exchange of gas and liquid momentums is governed not by MFR but by MR_{Lip}:

$$\frac{\lambda_{Lon}}{D_{Lip}} = \frac{c}{\sqrt{MR_{Lip}}} \tag{9}$$

where c is the constant.

Since the liquid sheet is atomized within an extremely short distance from the injector, it is not easy to measure λ_{Lon} from experimental images. On the other hand, it is easy to measure the oscillation frequency f_{Lon} of the liquid sheet. The λ_{Lon} and f_{Lon} are determined physically far upstream of the point where the first wave appears. Even at the downstream point, the effect of V_G on wave velocity is 3~4 % [17]. That is why we ignore the acceleration of liquid sheet by the air flow in this study. Therefore, the oscillation frequency f_{Lon} of the liquid sheet can be given

by:

$$V_L = \mathrm{f}_{Lon}\lambda_{Lon} \tag{10}$$

Finally, we derive the following correlation on f_{Lon} from eqs. (9) and (10):

$$\mathrm{f}_{Lon} = \frac{c'V_G}{\sqrt{\rho_L/\rho_G}\sqrt{D_L D_{Lip}}} \tag{11}$$

where c' is the constant. The validity of the correlation on f_{Lon} is examined in this study.

3. Experimental Setup and Condition

Experiments with a planar air-blast atomizer were carried out with various fluid properties and injectors to understand the deformation and atomization characteristics and to examine the validity of the proposed correlations. Figures 1(a) and (b) show the experimental apparatus for atmospheric pressure test and that for high ambient pressure test, respectively. We used the same experimental rigs which were used by Yoshida et al. [4]. Filtered kerosene or water at room temperature was injected into the atmosphere or high ambient pressure through an injector, and filtered water with T_L = 283, 288, 323 K was also injected into the atmosphere to examine the effect of liquid viscosity μ_L. In the followings, unless otherwise noted, liquid temperature T_L was 288±5 K. The liquid was injected using a pump (Fuji Techno Industries, Co., HYSA-20) and liquid flow rate was adjusted by the rotation controller (Mitsubishi Electric Co., GM-S). The maximum error in measured V_L was 1 %. In the experiment of high water temperature, water in the liquid tank was heated by a heater (Kashima Co. Ltd., WPS-110, 1000W maximum) with a temperature controller. The heated water was injected continuously to warm up the piping system before the visualization test, so that hot water at the stable temperature of 323 K ±2 K was injected from the injector. We measured the temperature of injected water by a thermometer just after the injection. The air flow was injected from a blower (Kawasaki Heavy Industries, Ltd., GR91) or a compressor (Maximum discharge pressure was 1 MPa). The gas flow rate was controlled using a valve, and was measured using a manometer at the atmospheric pressure test rig and was measured using a flow meter at the high ambient pressure test rig. The maximum error in measured V_G was 2% .

Figures 2(a) and (b) show the side and bottom views of the injector exit. We performed backlight high-speed photographing via a high-speed camera (Vision Research Inc., Phantom v7.3) and a metal-halide lamp (Kyowa Co. Ltd., MID-25FC). The spatial resolution of the images was 90 μm / pixel, and the acquisition rate was 6,504 ~ 8,000 frames per second. Table 2 shows the entire experimental conditions, and Table 3 shows fluid properties of liquids at liquid temperature T_L=283, 288 and 323 K. Physical property of water is based on the database [18]. Physical property of kerosene was referred from the article [19]. When the temperature of pure water is changed from 283 to 323 K, liquid viscosity μ_L becomes less than half of the original value. On the other hand, the change in surface tension by the temperature variation from 283 K to 323 K is only 8 %. That is why the effect of the difference in surface tension is smaller than that of the difference in viscosity. Since air-blast atomizers are operated under high Weber number condition, the effect of surface tension on λ_{Lon} is not considered in the previous studies [11, 13, 14] and in this study.

Lip thickness D_{Lip} was 0.2 or 0.4 mm, and liquid sheet thickness D_L was 0.2 or 0.5 mm, and air channel width D_G was fixed to 3.0 mm. The ranges of gas velocity V_G were $15 < V_G < 75$ m/s and liquid inflow velocity V_L was

varied within $0.7 < V_L < 3.8$ m/s. Ambient pressure P_a was varied from 0.1 to 0.4 MPa. As shown in Fig. 3, we measured oscillation frequency f_{Lon} by FFT analysis of the time histories of the luminosity at the white rectangle region where the first waves were passing through. The frequency resolution was 25.4 Hz.

4. Results and Discussion

4.1 Visualization

Time histories of the front and side views of a flapping water sheet for V_L=1.2 m/s, V_G=30 m/s, P_a=0.1 MPa, D_L=0.5 mm and D_{Lip}=0.2 mm are shown in Fig. 4. The images of the front and side views were captured individually. The red lines showing wave undulations in front and side views correspond to each other. The liquid film has a smooth interface near the exit of the injector and oscillates largely in the downstream by the K-H instability theory. In this case at about 15 mm downstream of the injector, the rapture of the liquid sheet occurs after the bag formation induced by Rayleigh-Taylor instability [20-21]. Fernandez et al. [5] concluded that deformation pattern map of a planar liquid sheet could be governed by MFR, and cellular break-up [3] occurred when MFR was below 0.50. Figure 5 shows some front views of liquid sheets of kerosene and water sorted by MFR. Flow patterns and longitudinal wavelengths of kerosene and water are different even with the same MFR. As can be seen from Fig. 5 (b), Cellular break-up does not occur at V_L=0.75 m/s and MFR=0.7. Thus, it is confirmed that deformation pattern map cannot be summarized by MFR. In the followings, we arrange flow patterns and f_{Lon} based on V_G and V_L to clarify the dominant factors on the liquid sheet atomization process.

Figure 6 shows the images of the oscillating water sheet at various P_a to examine the effects of ρ_G. The longitudinal wavelength λ_{Lon} of the oscillating liquid sheet decreases with increasing V_G. The density ratio ρ_L/ρ_G is smaller at higher P_a, which decreases λ_{Lon} based on the K-H instability.

The front views of the water sheets with D_{Lip}=0.2, 0.4 mm and D_L=0.5, 0.2 mm are shown in Figs. 7(a) and (b), respectively. The wavelength at D_{Lip}=0.4 mm is slightly longer than that for D_{Lip}=0.2 mm.

We have reported that gas and liquid viscosities do not largely affect the oscillation of a liquid sheet at several hundred of liquid Reynolds number [12]. In this study, we performed the experiment with various water temperatures T_L in order to clarify whether we can neglect the effect of μ_L, in other word, the effect of δ_L, on the liquid sheet oscillation under the wide range of experimental conditions. Figure 8 shows the images of the oscillating liquid sheets with T_L=283 K and 323K. When the temperature is changed from 283 to 323 K, μ_L decreases from $1.3\text{x}10^{-3}$ to $5.5\text{x}10^{-4}$ Pa・s. The liquid sheet patterns at different μ_L are extremely similar in spite of the large difference in μ_L.

4.2 Oscillation frequency f_{Lon}

Figure 9 shows measured f_{Lon} with kerosene and water, by which the effects of liquid density ρ_L can be examined. Oscillation frequency f_{Lon} for kerosene is in proportion to V_G, which shows the same trend as water, and f_{Lon} of kerosene is higher than that of water at same V_G. The measured f_{Lon} shown in Fig. 9 does not depend on V_L. Figure 10 shows the side views of a water sheet. The λ_{Lon} increases with liquid velocity V_L. The fact indicates that wave velocity is nearly equal to V_L. The interaction between gas and liquid is promoted by increasing V_G. Squire [2] and Park et al. [22] proposed the following equation based on the inviscid linear instability theory:

$$\lambda_{Lon} \approx \frac{4\pi\sigma}{\rho_G(V_G - V_L)^2} \quad (12)$$

Villermaux [13] and Marmottant & Villermaux [14] proposed the following correlation on λ_{Lon}:

$$\lambda_{Lon} \sim \frac{5.6}{1.5}\frac{2\pi}{\rho_G}\sqrt{\frac{\rho_L \mu_G D_G}{V_G}} \quad (13)$$

According to eq. (12), λ_{Lon} is in inverse proportion to $(V_G - V_L)^2$. However, our experimental result shows that λ_{Lon} is not inversely proportional to V_G^2 but V_G due to the effect of the wake of the lip. In eq. (13), the effects of D_G and μ_G are taken into account while the effects of D_L, D_{Lip} and V_L are not taken into account. The liquid sheet in an air-blast atomizer is thin whose thickness is of the order of 100 μm while the liquid in a coaxial injector is thick whose thickness is of the order of 1 mm. The difference between eq. (9) and eq. (13) may be caused by the difference in the thicknesses of the liquid. From the above discussions, we can conclude that conventional theoretical analysis without the lip is not applicable to predict λ_{Lon}.

Figure 11 shows measured f_{Lon} for various P_a, which represents the effects of ρ_G. The result clearly shows that the higher ρ_G results in higher f_{Lon}, which agrees with the trend obtained by eq. (11). The oscillation frequencies f_{Lon} obtained by the present experiment with various D_L and D_{Lip} are presented in Fig. 12. It is clear that the smaller D_L is, the larger f_{Lon} becomes, which agrees qualitatively with Lozano's result [11]. The result also indicates that the increase in D_{Lip} decreases f_{Lon}. Measured frequencies f_{Lon} with different temperatures of 283K and 323K are shown in Fig. 13. The result for hot water agrees well with that for cold water, by which we can clearly conclude that the effect of μ_L on f_{Lon} is ignorable.

4.3 Validation of correlations of f_{Lon} and λ_{Lon}

Finally, we verify the validity of correlations on f_{Lon} and λ_{Lon} using the measurement data. By using a least squares method, we fit the experimental result to our correlation. Figure 14 shows the relationship between measured $\sqrt{\rho_L/\rho_G}\sqrt{D_L D_{Lip}} f_{Lon}$ and V_G for all the experimental data. The result confirms that the effects of fluid properties and injector geometries on f_{Lon} can be correlated well by eq. (11) with c' = 0.095 whose asymptotic standard error (ASE) is 1.2 %. Hence, we can obtain the following correlation.

$$\sqrt{\rho_L/\rho_G}\sqrt{D_L D_{Lip}} f_{Lon} = 0.095 V_G \quad (14)$$

At high V_G, measured f_{Lon} obtained at the atmospheric pressure test rig becomes slightly higher than that obtained at the high ambient pressure test rig because of the spatial constraint in the high ambient pressure test rig. Hence, measured f_{Lon} for V_G>40 m/s in the atmospheric pressure test is slightly larger than the prediction.

Figure 15 shows the comparison between our measured result and the prediction using the correlation eq. (3) proposed by Lozano et al. [11]. Their correlation overestimates the wavelength and cannot appropriately take into account the effect of the injector geometry. Figure 16 shows the relationship between measured λ_{Lon}/D_{Lip} and $1/\sqrt{MR_{Lip}}$ for all the experimental data. These results agree well with the newly proposed correlation given as equation (9) with c=14.3 and ASE=1.7%, which confirms the validity of the proposed correlation on λ_{Lon}. From the results, the dimensionless relation between λ_{Lon} and MR_{Lip} by considering dominant fluid properties and injector geometries is given as follows:

$$\frac{\lambda_{Lon}}{D_{Lip}} = \frac{14.3}{\sqrt{MR_{Lip}}} \quad (15)$$

From this study, it is found that f_{Lon} and λ_{Lon} depend on lip thickness, and it is important to pay attention to the lip thickness in the design of an air-blast atomizer.

5. Conclusions

The longitudinal oscillation of a planar liquid sheet induced by air flows with various liquid densities ρ_L, gas densities ρ_G, liquid velocities V_L, gas velocities V_G, liquid viscosities μ_L, liquid sheet thicknesses D_L and lip thicknesses D_{Lip} was investigated. Firstly, we proposed the new correlations on the longitudinal wavelength λ_{Lon} and frequency f_{Lon} based on the previous studies. Then, we visualized the planar oscillating liquid sheet with parallel air flows, and obtained the additional experimental data with various V_G and μ_L to cover all the effects of fluid properties and injector geometries on the deformation and atomization characteristics of the oscillating liquid sheet. Finally, the correlations on λ_{Lon} and f_{Lon} were verified using our entire measurements. As a result, we obtained the following conclusions.

(1) Deformation pattern map of a liquid sheet with air flows cannot be summarized by MFR.

(2) The effects of μ_L on f_{Lon} and λ_{Lon} are ignorable under the present experimental condition.

(3) We proposed the lip momentum ratio MR_{Lip} as a new dominant dimensionless number based on the lip thickness D_{Lip}, since the thickness of the gas velocity boundary layer at the downstream of the lip depends on D_{Lip}.

(4) We derived the correlation on λ_{Lon} given by $\frac{\lambda_{Lon}}{D_{Lip}} = \frac{14.3}{\sqrt{MR_{Lip}}}$ and that on f_{Lon} given by $f_{Lon} = \frac{0.095V_G}{\sqrt{\rho_L/\rho_G}\sqrt{D_L D_{Lip}}}$, whose validities were verified through the comparison between measured and estimated results.

Acknowledgements

Visualizations experiments were performed using the experimental apparatus at Japan Aerospace Exploration Agency (JAXA). Present authors would like to express gratitude to Associate Senior Researcher, Dr. Kazuaki Matsuura, of JAXA for his warm support and kind comments.

References

[1] Lefebvre A. H. Airblast Atomization: Progress in Energy and Combustion Science 1980;6:233-261.

[2] Squire H. B. Investigation of the Instability of a Moving Liquid Film: British Journal of Applied Physics 1953;4(6):167-169.

[3] Stapper B. E., Samuelsen G. S. An Experimental Study of the Breakup of a Two-dimensional Liquid Sheet in the Presence of Co-flow Air Shear: 28th AIAA Aerospace Sciences Meeting;1990-0461, 1990.

[4] Yoshida K., Ide K., Matsuura K., Iino J., Kurosawa Y., Hayashi S., and Ohta Y. Airblast Spray Characteristics of Planar Liquid Films in Longitudinal Gas-Phase Shear Layers at Various Ambient Pressure Conditions: Proceedings of the 12th International Conference on Liquid Atomization and Spray Systems (Heidelberg, Germany), 2012.

[5] Fernandez V., Berthoumieu P., and Lavergne G. Primary Atomization in Water and Kerosene Liquid Sheets at High Pressure: Proceedings of the 11th International Conference on Liquid Atomization and Spray Systems (Colorado, United States), 2009.

[6] Dejean B., Berthoumieu P., Gajan P. Experimental Study on the Influence of Liquid and Air Boundary Conditions on a Planar Air-Blasted Liquid Sheet, Part I: Liquid and Air Thicknesses: International Journal of Multiphase Flow 2016;79:202-213.

[7] Villedieu P., Blanchard G., Zuzio D. Numerical Simulation of Primary Atomization of a Sheared Liquid Sheet. Part2: Comparison with Experimental Results: Proceedings of the 25th ILASS-Europe (Chania, Greece), 2013.

[8] Li-zi Q., Ran Y., Li-jun Y. Theoretical Breakup Model in the Planar Liquid Sheets Exposed to High-Speed Gas and Droplet Size Prediction: International Journal of Multiphase Flow 2018;98:158-167.

[9] Senecal P.K., Schmidt D.P., Nouar I., Rutland C.J., Reitz, R.D., Corradini, M.L. Modeling High Speed Viscous Liquid Sheet Atomization: International Journal of Multiphase Flow 1999;25:1073–1097 .

[10] Li X., Tankin R.S., On the Temporal Instability of a Two-Dimensional Viscous Liquid Sheet: Journal of Fluid Mechanics 1991;226:425-443.

[11] Lozano A., Barreas F., Siegler, C., Low D. The Effects of Sheet Thickness on the Oscillation of an Air-blasted Liquid Sheet: Experimental in Fluids 2005;39(1):127-139.

[12] Oshima I., Sou A. Numerical Simulation of Liquid Sheet Deformation Caused by Air Flow: Transactions of the Japan Society for Aeronautical and Space Sciences, Aerospace Technology Japan 2018;16(4):319-327.

[13] Villermaux E. Mixing and Spray Formation in Coaxial Jets: Journal of Propulsion and Power 1998;14(5):807-817.

[14] Marmottant P., Villermaux E. On Spray Formation: Journal of Fluid Mechanics 2004;498:73–111.

[15] Oshima I., Sou A., Kawabata R., Matsuura K. Longitudinal Wavelength of Oscillating Liquid Sheet with Air Flow: 55th AIAA Aerospace Sciences Meeting; 2017-1464, 2017.

[16] Villermaux E. On the Role of Viscosity in Shear Instabilities: Physics of Fluids 1998;10(2):368-373.

[17] Oshima I., Sou A., Matsuura K. Numerical and Experimental Study on Liquid Sheet Deformation by Air Flow: Proceedings of the 13th. ICLASS (Tainan, Taiwan), 2015.

[18] The National Institute of Advanced Industrial Science and Technology in Japan. Network Database System for Thermophysical Property Data, https://tpds.db.aist.go.jp/index_en.html; 2018 [accessed 11 July 2018].

[19] Zheng Q. P., Jasuja A. K., Lefebvre A. H. Structure of Airblast Sprays Under High Ambient Pressure Conditions: Journal of Engineering for Gas Turbines and Power 1997:119(3):512-518.

[20] Rayleigh Lord. Investigation of the Character of the Equilibrium of an Incompressible Heavy Fluid of Variable Density: Proceedings of the Royal Society of London 1883;14:170-177.

[21] Taylor G. I. The Instability of Liquid Surfaces when Accelerated in a Direction Perpendicular to their Plane.I: Proceedings of the Royal Society of London 1950;201:192-196.

[22] Park J., Huh K. Y., Li X., Renksizbulut M. Experimental Investigation on Cellular Breakup of a Planar Liquid Sheet from an Air-Blast Nozzle: Physics of Fluids 2004;16(3):625–632.

Table 1. Correlations on the longitudinal wavelength λ_{Lon} of the liquid

Author	Lozano et al. [11]	Marmottant et al. [14]	Squire [2]
Characteristics	Air-blasted planar liquid sheet	Liquid jets in a coaxial air stream	Thin liquid in a stationary gas
Condition	$0.5<D_L<1.9$ mm, $3.45<D_G<35$ mm	$V_G>>V_L$, large We, $D_{Lip}=1.6$ mm	Low ambient pressures
Wavelength	$\frac{\lambda_{Lon}}{\sqrt{D_L D_G}}=\frac{20.39}{\sqrt{MR}}$	$\lambda_{Lon}\cong\frac{2\pi}{1.5}\left(\frac{\rho_L}{\rho_G}\right)^{1/2}\delta_G$	$\lambda_{Lon}=\frac{4\pi\sigma}{\rho_G V_L^2}$

Author	Oshima et al. [12]	Villermaux [13]
Characteristics	2D liquid sheet with air flows	Liquid jets in a coaxial air stream
Condition	$D_{Lip}=0$, 0.4 mm, $D_L=0.5$mm	$\rho_L>>\rho_G$, $V_G>>V_L$
Wavelength	$\lambda_{Lon}\propto\frac{1}{\sqrt{MFR}}$	$\lambda_{Lon}=3\pi(\sigma/\rho_G V_G^2)$

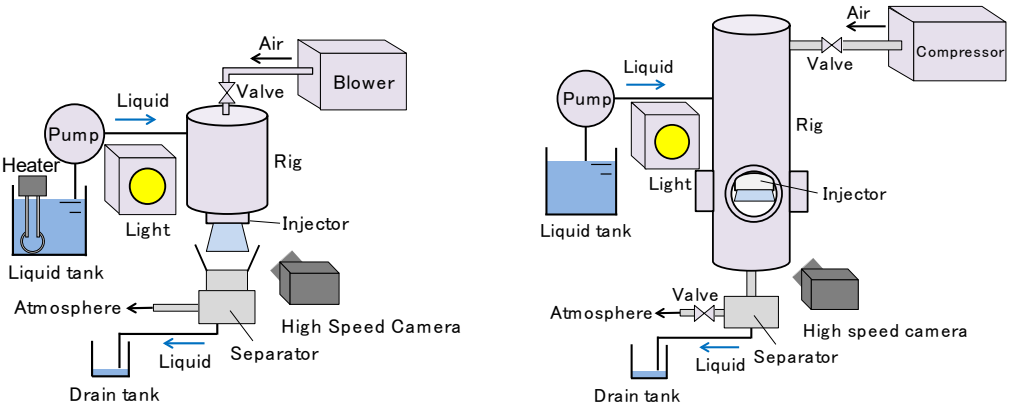

(a) Atmospheric pressure test rig (b) High ambient pressure test rig

Fig. 1. Experimental set up

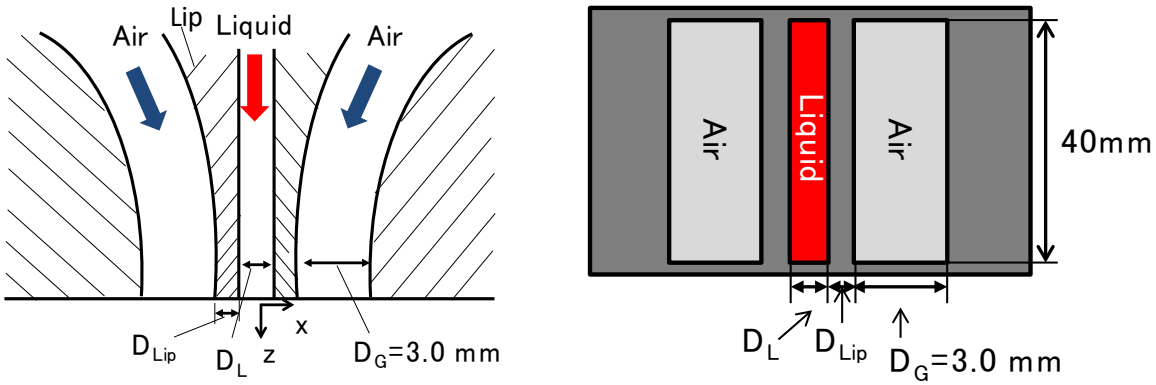

(a) Side view (b) Top view

Fig. 2. Schematic of planar air-blast atomizer

Table 2. Experimental condition

Parameter	Values	Parameter	Values
Lip thickness D_{Lip} [mm]	0.2, 0.4	Ambient pressure P_a [MPa]	0.1, 0.15, 0.2, 0.3, 0.4
Liquid sheet width D_L [mm]	0.2, 0.5	Gas velocity V_G [m/s]	$15 < V_G < 75$
Air channel width D_G [mm]	3.0	Liquid velocity V_L [m/s]	$0.7 < V_L < 3.8$
Liquid temperature T_L [K]	283, 288, 323		

Table 3. Fluid properties of liquids [17, 18]

Liquid (T_L=288 K)					
Water			Kerosene		
Density ρ [kg/m^3]	Viscosity μ [mPa·s]	Surface tension σ [mN/m]	Density ρ [kg/m^3]	Viscosity μ [mPa·s]	Surface tension σ [mN/m]
999	1.1	74	784	1.3	28

Water					
T_L=283 K			T_L=323 K		
Density ρ [kg/m^3]	Viscosity μ [mPa·s]	Surface tension σ [mN/m]	Density ρ [kg/m^3]	Viscosity μ [mPa·s]	Surface tension σ [mN/m]
1000	1.3	74	988	0.5	68

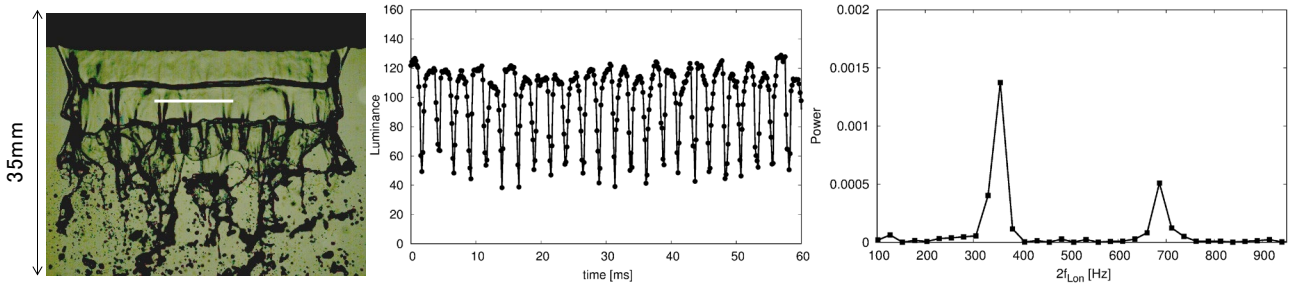

(a) Measured region (b) Time history of the brightness (c) Power spectrum of the brightness

Fig. 3. A sample of FFT analysis to calculate oscillation frequency f_{Lon}

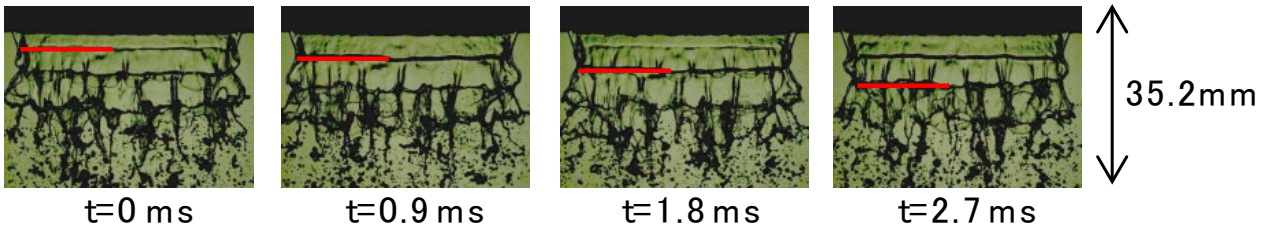

(a) Front view

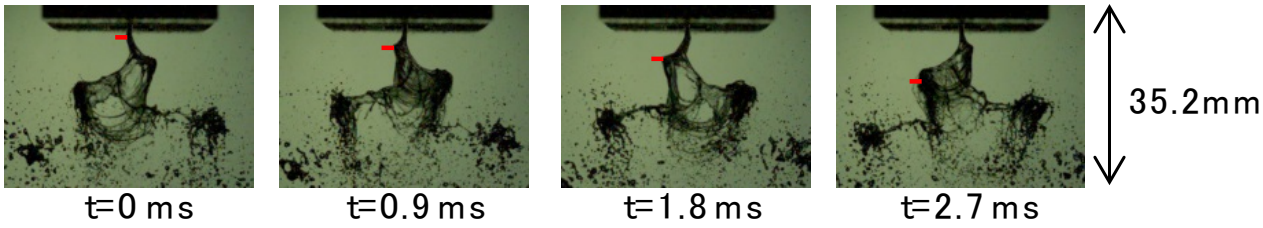

(b) Side view

Fig. 4. High-speed images of water sheet (V_L=1.2 m/s, V_G=30 m/s, atmospheric pressure, D_L=0.5 mm, D_{Lip}=0.2 mm)

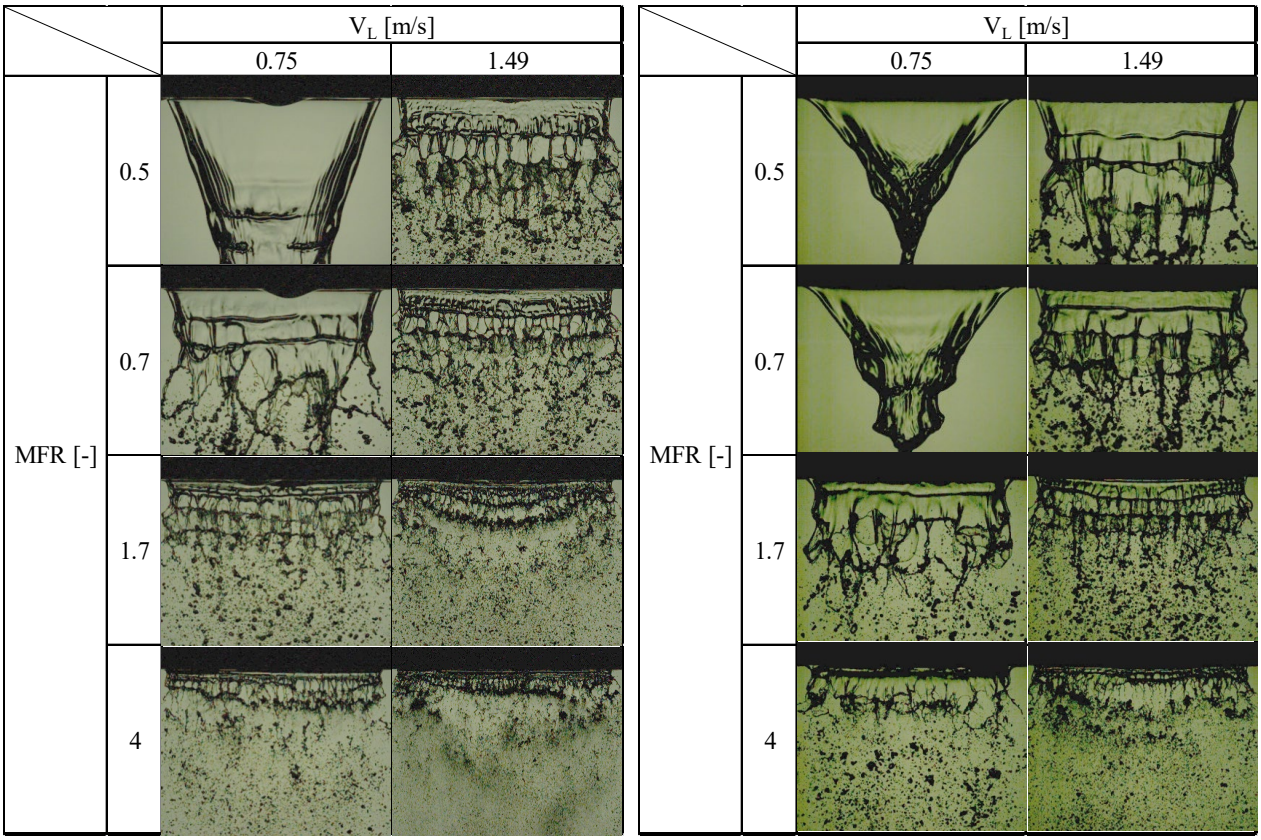

(a) Kerosene (b) Water

Fig. 5. Flow patterns of kerosene and water based on momentum flux ratio

(atmospheric pressure, D_L=0.5 mm, D_{Lip}=0.2 mm)

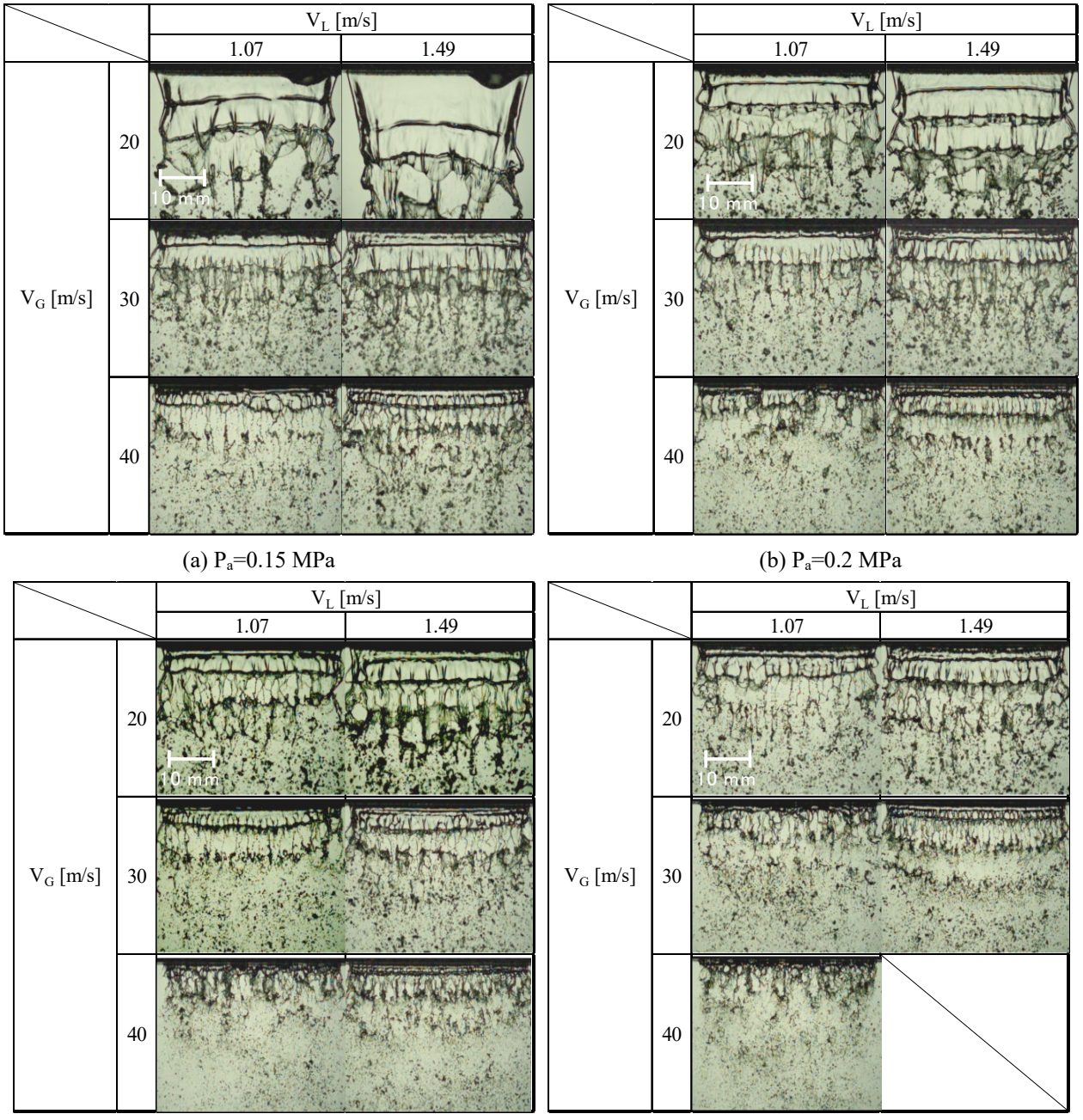

(a) P_a=0.15 MPa

(b) P_a=0.2 MPa

(c) P_a=0.3 MPa

(d) P_a=0.4 MPa

Fig. 6. Effect of ambient pressure P_a on flow pattern of water sheet (D_L=0.5 mm, D_{Lip}=0.2 mm)

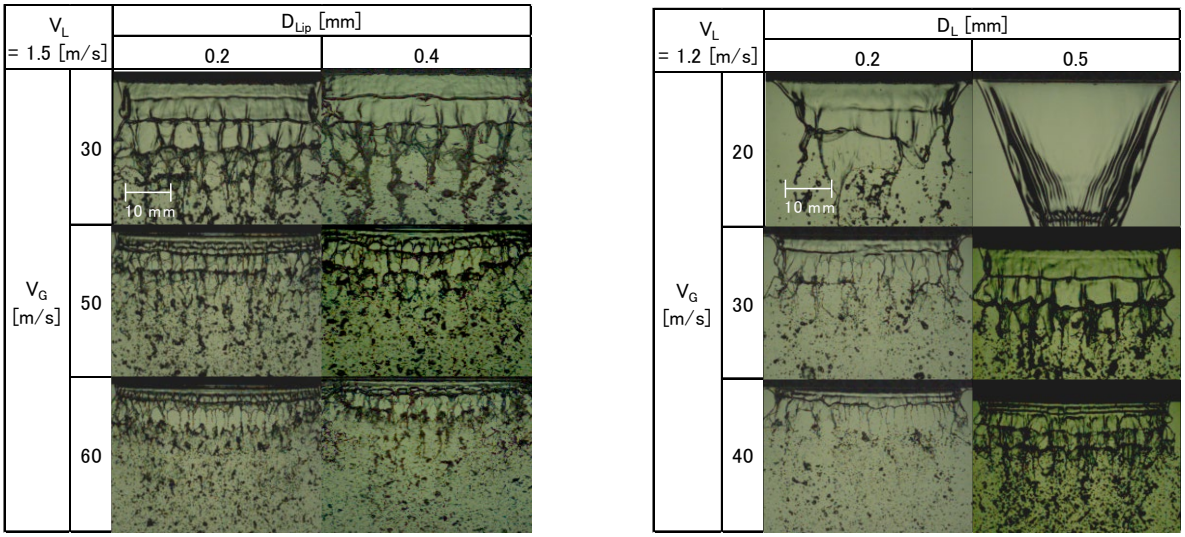

(a) Effect of D_{Lip} (D_L=0.5 mm) (b) Effect of D_L (D_{Lip}=0.2 mm)

Fig. 7. Effects of D_{Lip} and D_L on flow pattern of water sheet (atmospheric pressure)

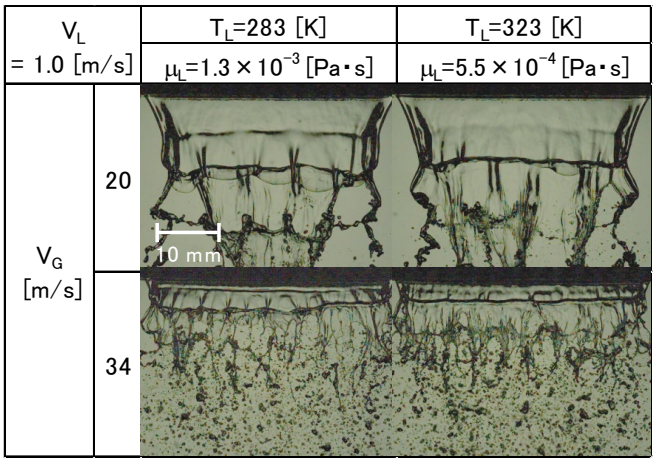

Fig. 8. Effect of T_L on flow patterns of water sheet (atmospheric pressure, D_L=0.5 mm, D_{Lip}=0.2 mm)

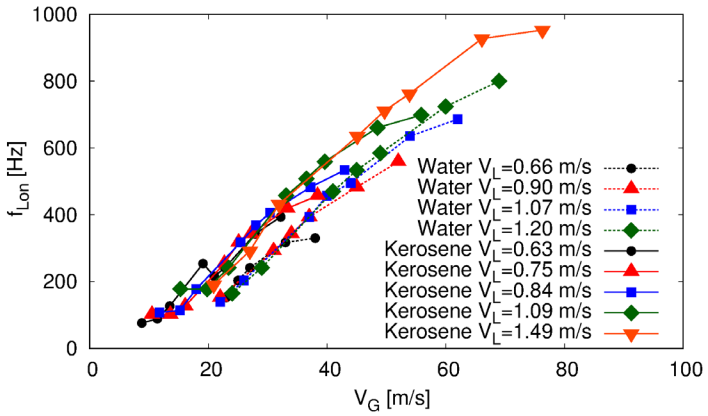

Fig. 9. Effect of ρ_L on longitudinal wavelength λ_{Lon} (atmospheric pressure, D_L=0.5 mm, D_{Lip}=0.2 mm)

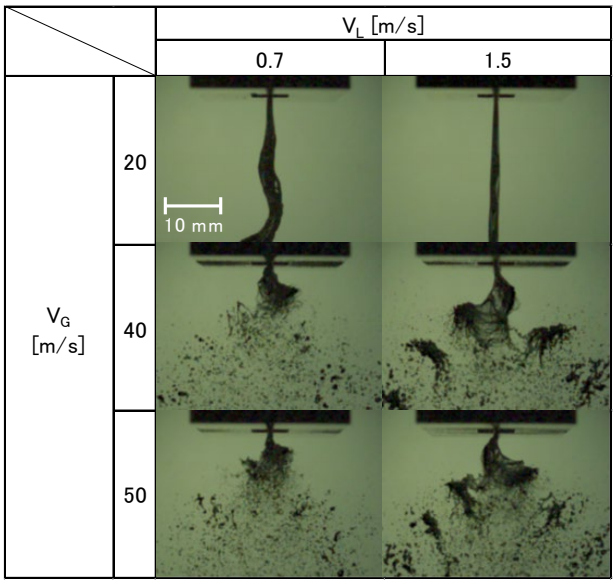

Fig. 10. Side views of water sheet to show the effect of V_L on λ_{Lon} (atmospheric pressure, D_L=0.5 mm, D_{Lip}=0.2 mm)

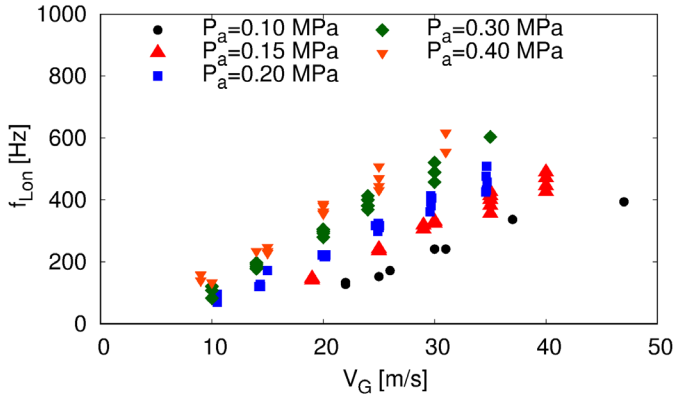

Fig. 11. Effect of gas density ρ_G on f_{Lon} (Water, D_L=0.5 mm, D_{Lip}=0.2 mm)

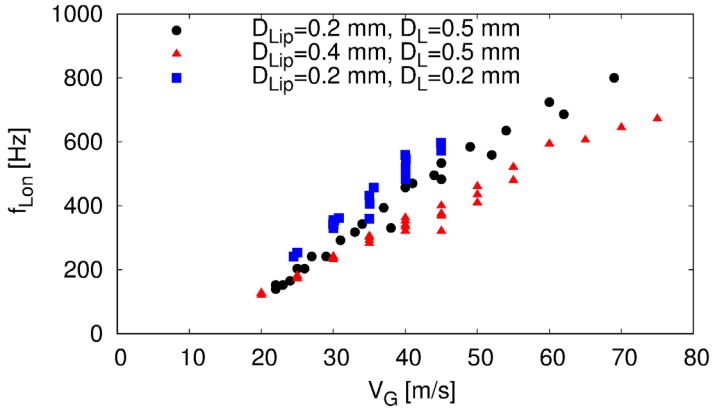

Fig. 12. Effects of D_{Lip} and D_L on f_{Lon} (Water, atmospheric pressure)

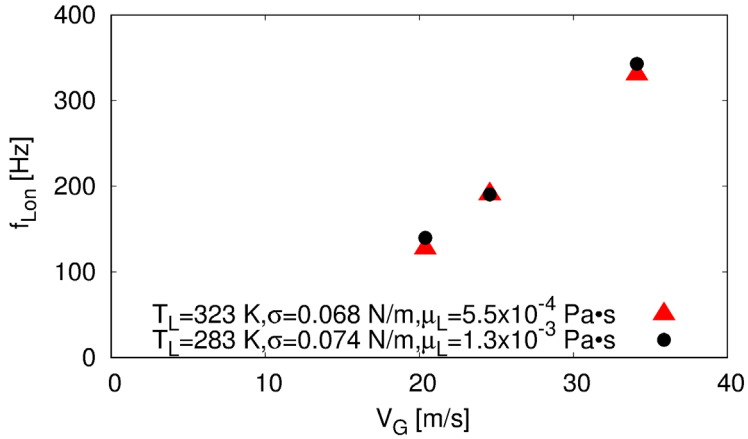

Fig, 13. Effect of T_L on f_{Lon} (Water, atmospheric pressure, D_L=0.5 mm, D_{Lip}=0.2 mm)

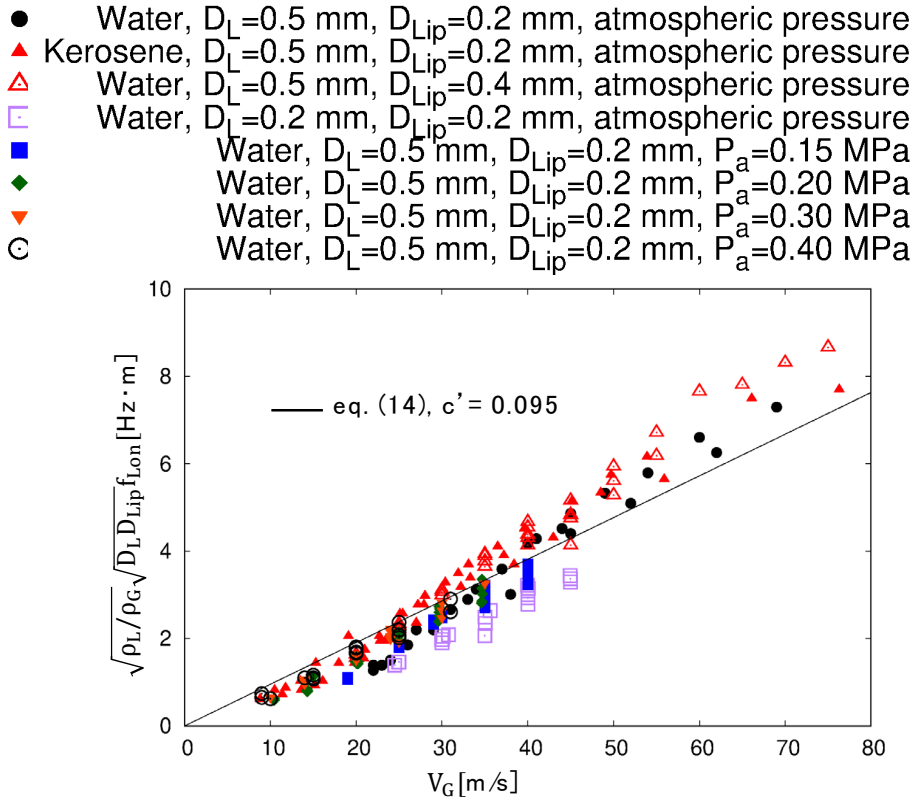

Fig. 14. Normalized frequency taking into account all experimental data

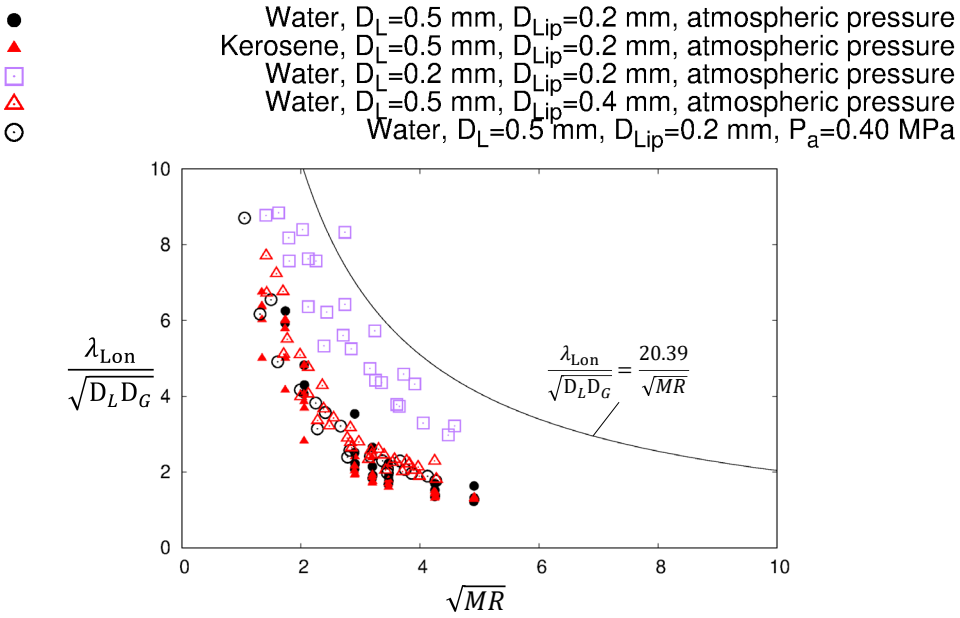

Fig. 15. Comparison of our experimental result and Lozano's correlation

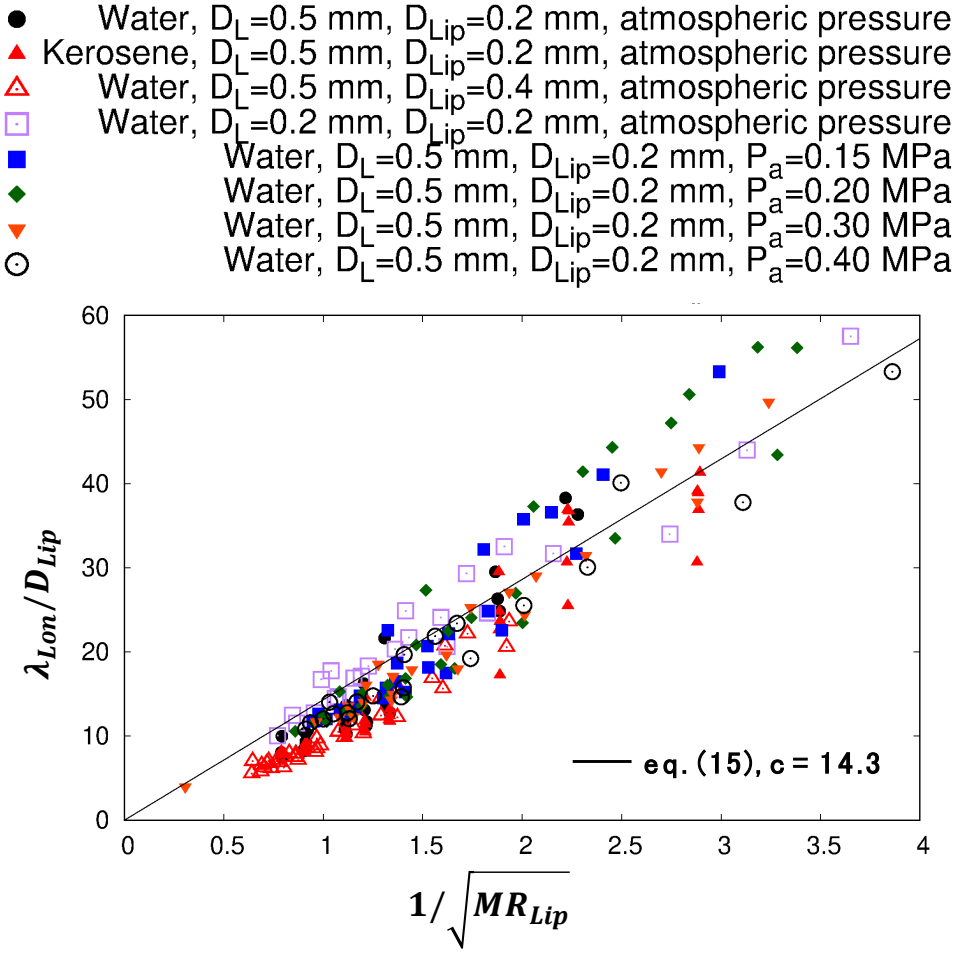

Fig. 16. Non-dimensional wavelength λ_{Lon} / D_{Lip} with lip momentum ratio MR_{Lip}